Nickel(II) complexes with methyl(2-pyridyl)ketone oxime: Synthesis, crystal structures and DFT calculations

ARTICLE *in* SPECTROCHIMICA ACTA PART A MOLECULAR AND BIOMOLECULAR SPECTROSCOPY · DECEMBER 2012

Impact Factor: 2.35 · DOI: 10.1016/j.saa.2012.12.042 · Source: PubMed

7 AUTHORS, INCLUDING:

Lorena Martinez Geribón
University of the Republic, Uruguay
1 PUBLICATION **4** CITATIONS
SEE PROFILE

Jorge S. Gancheff
University of the Republic, Uruguay
45 PUBLICATIONS **337** CITATIONS
SEE PROFILE

Robert Burrow
Universidade Federal de Santa Maria
115 PUBLICATIONS **923** CITATIONS
SEE PROFILE

Raul Chiozzone
University of the Republic, Uruguay
25 PUBLICATIONS **410** CITATIONS
SEE PROFILE

Spectrochimica Acta Part A: Molecular and Biomolecular Spectroscopy 105 (2013) 439–445

Contents lists available at SciVerse ScienceDirect

Spectrochimica Acta Part A: Molecular and Biomolecular Spectroscopy

journal homepage: www.elsevier.com/locate/saa

Nickel(II) complexes with methyl(2-pyridyl)ketone oxime: Synthesis, crystal structures and DFT calculations

Lorena Martínez [a], Jorge S. Gancheff [a], F. Ekkehardt Hahn [b], Robert A. Burrow [c], Ricardo González [a], Carlos Kremer [a], Raúl Chiozzone [a,*]

[a] Cátedra de Química Inorgánica, Departamento Estrella Campos, Facultad de Química, Universidad de la República, Avda. General Flores 2124, CC 1157 Montevideo, Uruguay
[b] Institut für Anorganische und Analytische Chemie der Westfälischen Wilhelms-Universität Münster, Correnstrasse 30, 48149 Münster, Germany
[c] Departamento de Química, Universidade Federal de Santa Maria, Camobi, CEP 97105-900, Santa Maria, RS, Brazil

HIGHLIGHTS

- Three mononuclear Ni(II) complexes with mpkoH have been isolated and characterized.
- Their structural and electronic properties were also studied by DFT methods.
- Their electronic spectra have been reproduced by the TD-B3LYP/LANL2DZ method.

GRAPHICAL ABSTRACT

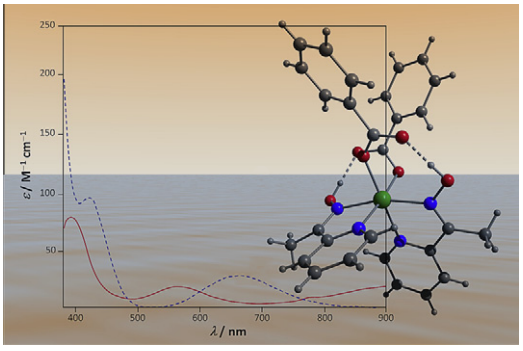

ARTICLE INFO

Article history:
Received 29 September 2012
Received in revised form 11 December 2012
Accepted 14 December 2012
Available online 22 December 2012

Keywords:
Nickel(II) complexes
Oxime complexes
Crystal structure
Theoretical calculations

ABSTRACT

The synthesis and structural characterization of the three novel nickel(II) complexes $[Ni(OOCPh)_2(mpkoH)_2]$ (**1**), $[Ni(NO_3)_2(mpkoH)_2]$ (**2**) and $[Ni(mpkoH)_3](NO_3)_2{\cdot}½H_2O$ (**3**·$½H_2O$), with mpkoH = methyl(2-pyridyl)ketone oxime is reported. Geometry optimization and population analyses were performed by means of DFT calculations for the previously mentioned compounds as well as for $[NiCl_2(mpkoH)_2]$ (**4**). Electronic UV–vis spectra were also simulated in the TD-DFT framework to assign the origin of the absorption bands and in doing so, to have a clear picture of the absorptive features of the coordination compounds under investigation.

Introduction

Oximes have been known for a long time as spectrophotometric reagents in analytical chemistry [1], and first reports on methyl(2-pyridyl)ketone oxime (mpkoH) were dealing with the colorimetric determination of iron, copper and rhenium [2,3]. This compound belongs to the family of 2-pyridyl oximes, of general formula (py)(R)C=N=OH with py = pyridine and R = H, alkyl or aryl group.

In the last decade, 2-pyridyl oximes became very popular ligands in molecular magnetism. This is due to their ability to form polynuclear complexes by acting as versatile and flexible bridging ligands that efficiently mediate magnetic exchange between paramagnetic ions. Several nickel(II) complexes with these ligands have been reported, mostly with 2-pyridinealdoxime (paoH), phenyl (2-pyridyl)ketone oxime (ppkoH) and mpkoH. Trinuclears $[Ni_3(ppko)_6]{\cdot}2H_2O{\cdot}0.5EtOH{\cdot}MeOH$ and $[Ni_3(mpko)_3(HCO_2)_2(mpkoH)_2]$

* Corresponding author. Tel.: +598 2924 9739; fax: +598 2924 1906.
E-mail address: rchiozzo@fq.edu.uy (R. Chiozzone).

1386-1425/$ - see front matter © 2012 Elsevier B.V. All rights reserved.
http://dx.doi.org/10.1016/j.saa.2012.12.042

(ClO_4) [4], hexanuclears $[Ni_6(SO_4)_2(ppko)_8]\cdot 6DMF$ [5], $[Ni_6(SO_4)_4(OH)(mpko)_3(mpkoH)_3(MeOH)_2(H_2O)]$ and $[Ni_6(SO_4)_4(OH)(ppko)_3(ppkoH)_3(MeOH)_3]$ [6], and the tetradecanuclear cluster $[Ni_{14}(OH)_4(N_3)_8(pao)_{14}(paoH)_2(H_2O)_2](ClO_4)_2$ [7] are some examples of nickel compounds that have been synthesized and fully characterized, structurally and magnetically. In addition, heteropolynuclear compounds such as $[NiTb(mpko)_2(NO_3)_3(mpkoH)]$, $[Ni_2Tb(mpko)_6](NO_3)$ and $[Ni_2Ln_2(mpko)_6(NO_3)_4]$ (Ln = Dy, Tb) have been obtained from the mononuclear precursor $[Ni(mpko)_2(mpkoH)]$ in a complex-as-ligand approach [8]. The high-nuclearity spin cluster $[Ni_8Dy_8O(OH)_4(pao)_{28}](ClO_4)_5(NO_3)$ is a nice example of 3d/4f molecule that exhibits slow magnetization relaxation [9].

Oximes can be easily deprotonated by addition of base and their ligand properties can be significantly altered in this way. In fact, all of the polynuclear complexes listed above were obtained when an external base was added to the reaction media.

On the contrary, only the dinuclear complex $[Ni_2(SO_4)_2(ppkoH)_4]$ and the mononuclear complexes $[Ni(ppkoH)_3](SO_4)$ [10], $[Ni(SO_4)(mpkoH)(H_2O)_3]\cdot H_2O$, $[Ni(SO_4)(mpkoH)_2(H_2O)]\cdot H_2O$ [11], $[NiBr_2(mpkoH)_2]$, $[Ni(mpkoH)(mpko)(H_2O)_2](NO_3)$ [12], $[NiCl_2(paoH)_2]$ and $[NiCl_2(mpkoH)_2]$ [13] have been obtained in absence of added base. Interestingly, the latter two compounds were recently found to be selective ethylene dimerization catalysts [13].

In spite of the several papers dedicated to the synthesis and characterization of nickel oxime complexes, as far as we know, no density functional theory (DFT) based calculations on their electronic spectral properties have been performed. In this study, we report the synthesis, structural and spectroscopic characterization of three novel nickel complexes bearing the mpkoH ligand, namely $[Ni(OOCPh)_2(mpkoH)_2]$ (**1**), $[Ni(NO_3)_2(mpkoH)_2]$ (**2**) and $[Ni(mpkoH)_3](NO_3)_2\cdot ½H_2O$ (**3**·½H_2O). Geometry optimization and population analysis were performed by means of DFT calculations for the further understanding of geometric and electronic properties of the complexes. Electronic UV–vis spectra were simulated in the TD-DFT framework to assign the origin of the absorption bands. The previously reported $[NiCl_2(mpkoH)_2]$ (**4**) was also theoretically investigated for comparison purposes.

Experimental

General procedures

The ligand mpkoH was prepared following a published procedure [14]. All other reagents and solvents were purchased from commercial sources and were used as received.

Elemental analyses for carbon, hydrogen and nitrogen were performed on a Carlo Erba EA1108 analyzer. IR spectra were recorded on a BOMEM MB 102 FT-IR spectrometer as KBr pellets, and UV–vis spectra were measured on a Shimadzu UV-1603 spectrophotometer.

Syntheses

*$[Ni(OOCPh)_2(mpkoH)_2]$ (**1**)*

NaOOCPh (1 mmol, 144 mg) and mpkoH (1 mmol, 136 mg) were added to a solution of $Ni(NO_3)_2\cdot 6H_2O$ (1 mmol, 291 mg) in methanol (10 mL). The resulting green solution was stirred overnight at ambient temperature. By slow evaporation of the solvent, crystals of **1** suitable for X-ray diffraction were obtained as blue prisms in 50% yield. Selected IR bands [ν_{max}/cm^{-1}]: 3108 w, 3061 w, 1845 s(br), 1600 s, 1548 s, 1480 m, 1395 vs, 1328 m, 1298 w, 1257 m, 1143 s, 1099 m, 1071 s, 1047 w, 1026 w, 835 m, 793 m, 783 m, 723 s, 688 m, 676 s, 568 m, 464 s. UV–vis (CH_2Cl_2) [λ/nm ($\varepsilon/M^{-1}cm^{-1}$)]: 396 (81), 562 (21), 782sh (12). Elemental analysis (%) for $NiC_{28}H_{26}N_4O_6$: found, C 58.08, H 4.95, N 9.79; calculated, C 58.67, H 4.57, N 9.77.

*$[Ni(NO_3)_2(mpkoH)_2]$ (**2**) and $[Ni(mpkoH)_3](NO_3)_2\cdot ½H_2O$ (**3**·½H_2O)*

$Ni(NO_3)_2\cdot 6H_2O$ (1 mmol, 291 mg) and mpkoH (3 mmol, 408 mg) were dissolved in 10 mL of methanol and stirred overnight at ambient temperature. Afterwards, the orange solution was layered with Et_2O and allowed to stand undisturbed for a few weeks. Crystals suitable for X-ray diffraction of **2** and **3**·½H_2O were obtained directly as violet plates and orange prisms in 25% and 70% yield, respectively.

Selected IR bands for **2** [ν_{max}/cm^{-1}]: 3427 m, 3173 m, 3084 m, 3030 m, 2867 m, 1603 s, 1482 w (sh), 1438 vs, 1385 s, 1309 s, 1288 s, 1139 m, 1103 m, 1047 s, 966 w, 893 w, 821 w, 779 s, 748 w, 682 m, 645 w, 571 w, 468 w, 426 w. UV–vis (CH_3NO_2) for **2** [λ/nm ($\varepsilon/M^{-1}cm^{-1}$)]: 563 (12), 780sh (8). Elemental analysis (%) for $NiC_{14}H_{16}N_6O_8$: found, C 37,05, H 3,65, N 18,49; calculated, C 36,96, H 3,54, N 18,47.

Selected IR bands for **3**·½H_2O [ν_{max}/cm^{-1}]: 3401 m (br), 3198 m (br), 1600 s, 1481 w, 1384 s, 1329 m, 1258 w, 1162 w, 1139 w, 1100 w, 1063 w, 1037 s, 829 w, 781 s, 749 w, 681 m, 643 w, 570 w, 420 w. UV–vis (CH_3OH) for **3**·½H_2O [λ/nm ($\varepsilon/M^{-1}cm^{-1}$)]: 395 (55), 530 (6), 792 (5). Elemental analysis (%) for $NiC_{21}H_{24}N_8O_9$: found, C 42.37, H 4.70, N 18.33; calculated, C 42.67, H 4.09, N 18.96.

*$[NiCl_2(mpkoH)_2]$ (**4**)*

MpkoH (1 mmol, 136 mg) was added to a solution of $NiCl_2\cdot 6H_2O$ (1 mmol, 238 mg) in 10 mL of methanol. The resulting green solution was stirred overnight at ambient temperature. By slow evaporation of the solvent, crystals of **4** were obtained as green prisms in 75% yield. Selected IR bands [ν_{max}/cm^{-1}]: 3132 m, 3064 m, 3020 m, 2935 m, 2690 m, 1662 w, 1599 s, 1477 m, 1448 m, 1381 m, 1327 m, 1257 m, 1165 m, 1141 m, 1102 m, 1062 m, 1050 s, 1015 w, 970 m, 892 w, 783 s, 747 m, 704 s, 682 m, 642 m, 568 m, 478 w, 416 m. UV–vis (CH_2Cl_2) [λ/nm ($\varepsilon/M^{-1}cm^{-1}$)]: 575 (40). Elemental analysis (%) for $NiC_{14}H_{16}N_4O_2Cl_2$: found, C 41.52, H 3.99, N 13.62; calculated, C 41.84, H 4.01, N 13.94.

X-ray data collection and structure refinement

X-ray diffraction data were collected with a Bruker X8 Kappa APEX II CCD diffractometer equipped with a graphite monochromator and a Mo Kα sealed X-ray tube (λ = 0.71073 Å). Crystals were mounted on fine (*ca.* 100 μm) glass fibers with epoxy glue and data intensities were measured using 0.5° ω and φ scans to achieve at least four times multiplicity of observation. SAINT [15] was used to integrate the images using a narrow-frame algorithm giving the intensity data and the final cell parameters. Scaling and absorption correction using the multi-scan method was performed using TWINABS [16] for **1**, or SADABS [17] for **2** and **3**. The structures were solved and refined using the Bruker SHELXTL Software Package [18] on full-matrix least-squares using F^2. Hydrogen atoms on carbon atoms were positioned using geometric restraints. Hydrogen atoms in hydroxyl groups were refined allowing free torsional rotation and water molecules were refined as rigid groups. For **1**, the crystal was found to be non-merohedrally twinned in two components with the same cell parameters. Both components were integrated, the solution made with a crudely detwinned dataset and the final refinement made on both components (TWIN/HKLF 5). Crystal data, collection procedures and refinement results are summarized in Table 1.

Theoretical calculations

All theoretical investigations have been undertaken at the density functional level of theory (DFT). To conduct studies on equilibrium geometries, optimizations starting from molecular structures determined by X-ray crystallography were carried out, for which

Table 1
Crystal, X-ray collection and structure refinement data.

Compound	**1**	**2**	**3**·½H_2O
Chemical formula	$C_{28}H_{26}N_4NiO_6$	$C_{14}H_{16}N_6NiO_8$	$C_{42}H_{50}N_{16}Ni_2O_{19}$
Molecular weight	573.24	455.04	1200.40
Crystal size (mm^3)	0.16 × 0.23 × 0.42	0.14 × 0.15 × 0.34	0.09 × 0.33 × 0.49
Crystal color and habit	Violet prism	Violet prism	Orange plate
T (K)	100(1)	296(2)	296(2)
Crystal system	Triclinic	Monoclinic	Monoclinic
Space group	$P\bar{1}$	*Ia*	$P2_1/c$
Cell dimensions (Å, °)			
a	10.0149(4)	8.2935(3)	11.9191(6)
b	11.2619(5)	14.9892(6)	29.1813(11)
c	11.7052(5)	14.9452(7)	15.7018(6)
α	90.570(2)		
β	92.413(2)	90.668(2)	102.546(1)
γ	97.528(2)		
Volume ($Å^3$)	1307.49(10)	1857.76(13)	5330.9(4)
Z	2	4	4
ρ_{calc} (Mg m^{-3})	1.456	1.627	1.496
θ_{min}, θ_{max} (°)	1.74, 30.58	1.92, 30.62	1.75, 30.55
Reflections collected	76271	28617	65560
R_{int}, R_σ	2.99%, 2.45%	3.12%, 3.09%	4.29%, 5.35%
T_{min}, T_{max}	0.654, 0.746	0.650, 0.746	0.672, 0.746
Goodness-of-fit on F^2	1.034	1.022	1.038
Parameters, Data	363, 15236	267, 5411	727, 16104
R_1, wR_2 [I > 2σ(I)]	2.95%, 8.02%	2.90%, 6.66%	5.87%, 16.57%
R_1, wR_2 [all data]	3.28%, 8.20%	3.81%, 7.09%	11.80%, 19.67%
ρ_{min}, ρ_{max} (e^- $Å^{-3}$)	−0.314, 0.645	−0.218, 0.357	−0.813, 1.075

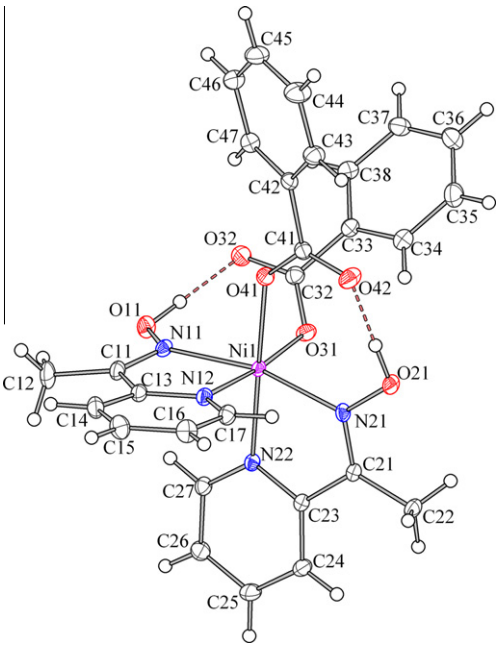

Fig. 1. Molecular structure and labeling for **1**. Ellipsoids are at 50% probability levels.

the triplet state (S = 1) was considered. PBE1PBE [19] in combination with the so-called STMIDI basis set showed to adequately describe geometries of large complexes [20–22] with a very low computational cost. The inclusion of PBE1PBE/STMIDI in this work was decided intending to expand the range of application of this methodology by testing its reliability in studying geometric and electronic aspect of complexes bearing different donor and metal atoms. The valence electrons for non-metal atoms in STMIDI were treated with MIDI! [23], those for the metal being described by a basis set (8s7p6d2f1g)/[6s5p3d2f1g] [24]. The core electrons were replaced by Stuttgart effective core pseudopotentials [24,25]. The nature of the stationary point was verified through a vibrational analysis (no imaginary frequencies).

The Time-Dependent DFT (TD-DFT) methodology was employed to calculate 100 vertical spin-allowed (50 = 50 singlet-triplet) transitions in the gas phase and in solution by means of B3LYP [26] in combination with LANL2DZ [27]. LANL2DZ and STMIDI take scalar relativistic effects into account, especially important when systems with transition metal atoms are studied [28]. The effect of the solvent was described by the conductor-like polarizable continuum model (C-PCM) [29], which is a valid model to consider the effects of the solvent as long as specific interactions between the solute and the solvent are not of significant importance. Electronic UV–vis spectra were simulated by means of the GaussSum software [30] considering all calculated transitions. Natural population analysis (NPA) calculations were performed with the NBO code [31] included in the program package Gaussian 03, Rev. D.02 [32], which has been used for all theoretical studies reported in this work.

Results and discussion

Description of the structures

The molecular structures of **1**, **2** and **3**·½H_2O show six-coordinated nickel(II) centers in slight distorted octahedral environments. In **1** and **2**, two neutral mpkoH oxime ligands chelate the nickel center *via* their nitrogen atoms. The remaining positions are occupied by two benzoato ligands for **1** (Fig. 1) or nitrato ligands for **2** (Fig. 2) coordinating via one oxygen atom in a *cis* arrangement, thereby forming a neutral coordination complex. The bis-chelate complexes are necessarily enantiomorphic. The crystallographic inversion center in **1** relates the Δ form in the figure to the Λ form, giving a racemic mixture with both enantiomers present in the crystal structure. Compound **2** crystallizes in the non-centrosymmetric space group *Ia* with a Flack parameter x = 0.021(10) [33] – the alternative to *Cc* was chosen to minimize the value of the cell angle β – indicating an enantiomorphically pure crystal in which the Λ form was observed for the selected crystal. Spontaneous resolution of enantiomorphic coordination compounds is well known [34]. In **3**·½H_2O, there are two crystallographically independent cationic complexes in the asymmetric unit, namely (I) and (II) (Fig. 3). In both of these, three neutral mpkoH ligands are coordinated *via* their nitrogen atoms in a chelating fashion to the nickel center in the *mer* configuration. The positive charges of the complex cations are balanced by four nitrate anions in the asymmetric unit. Additional electron density roughly corresponding to an isolated oxygen atom was found and modeled in the structure as a water molecule. Both complexes shown are in the Δ configuration. Crystallographic inversion centers generate the Λ configurations and the crystal structure is racemic.

Verification of the bond distances and angles of the complexes in the crystal structures with Mogul [35] showed no unusual values in any complex. The largest values for the z-scores are 1.404 (C41—O42) for **1**, 1.445 (Ni1—N12) for **2**, 1.334 (Ni1—N12) for **3**-(I), and 1.789 (Ni2—N42) for **3**-(II). Two nitrate anions in **3** show high z-score values most likely to unmodeled disorder as also seen by their large anisotropic thermal parameters. Selected bond distances and angles for **1**, **2** and **3** are given in Table 2.

The three crystal structures show hydrogen bonding of the oxime hydroxyl hydrogen atom (Table 3). In **1** and **2**, the hydrogen bonding is intramolecular to the free oxygen atoms of the bound anions. In **3**, the oxime hydroxyl hydrogen atoms form hydrogen bonds to the free nitrate anions.

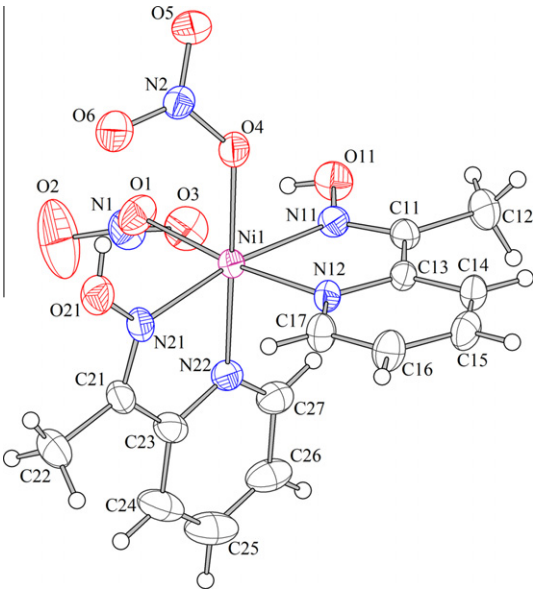

Fig. 2. Molecular structure and labeling for **2**. Ellipsoids are at 30% probability levels.

Geometry optimization, electronic structure and NPA results

Geometry optimization gave rise to a minimum as stationary point in all cases. All optimized structures exhibit the metal center residing in a slight distorted octahedral environment. Selected optimized parameters are presented in Table 4. The calculated geometries are in good agreement with the one observed from the crystallographic data.

Furthermore, it is worth mentioning that all optimized bis-chelate complexes showed the presence of the seven-membered-H-bond ring NOH···OX (X=C in **1**, N in **2**) and NOH···Cl (**4**) in line with the results from the X-ray diffraction studies. The PBE1PBE/STMIDI methodology was specially employed to obtain a good description of all the metric parameters involving the metal ion. In spite of this, PBE1PBE/STMIDI also leads the calculated bond lengths and angles in the rings —in the absence of counterions and crystal-packing-forces effects— to reasonably match the experimental data. For instance, OH···O distances of 1.30 and 1.48 Å and O—H···O angles of 178° and 168° have been calculated for **1** and **2**, respectively. The corresponding mean measured values are 1.60 and 1.88 Å, and 177 and 165°, respectively. For **4**, the OH···Cl length and the O—H···Cl angle were found to be 1.84 Å and 156°, the mean experimental values being 2.24 Å and 154°, respectively [13].

Calculated (NPA) charges on selected atoms are displayed in Table 5. The NPA result for nickel is smaller than the formal value of +2 as a result of the electron-density donation process. The metal ions feature charges ranging from +1.191 to +1.278, while the non-metals carry charges in the range from −0.154 to −0.708. For all complexes, the pyridine N atoms bear a higher charge than the oxime N atoms. It is worth mentioning that the presence of π-donor Cl^- ions in **4** results in a transferred density-charge which is more important than in the other complexes.

Electronic spectra

The electronic spectrum of **3** simulated in the presence of the solvent is displayed as an example in Fig. 4, which also includes the experimental one. The spectra for **1, 2** and **4** are depicted in the Supplementary Material (Figs. S1–S3). Calculated electronic transitions in the presence of the solvent for all complexes are presented in Tables 6 (**3**) and S1–S3 (**1**, **2** and **4**). In the high-energy part of the spectra, only transitions with oscillator strength (*f*) larger than 0.0020 were considered. For all electron excitations, only contributions larger than 15 % were taken into account. In all cases, no significant shifts were obtained in going from the gas phase to the solution.

One well-defined absorption band was simulated in the range 550–900 nm for all theoretically studied complexes. In all cases, the maximum of the absorption band were simulated red-shifted with respect to the experimental data, with displacements ranging from +94 nm for **1** to +115 nm for **2.** It can be noted a steady increase in the wavelength of the simulated maxima as the coordination environment changes from N_3O_3 in **3** (634 nm) to N_2O_4 in **1** and **2** (656 and 678 nm respectively) to $N_2O_2Cl_2$ in **4** (689 nm), in line with the progressive decrease in the ligand field strength. The experimental evidence suggests the presence of an absorption band beyond 900 nm. Also a shoulder at about 800 nm (except for **4**) is observed, which originates from the spin-forbidden transition to the ^1E_g singlet term. This finding is in line with the absorptive features displayed by nickel(II) complexes in octahedral coordination environment [36]. Neither the lowest-energy band nor the shoulder has been detected in the simulated spectrum.

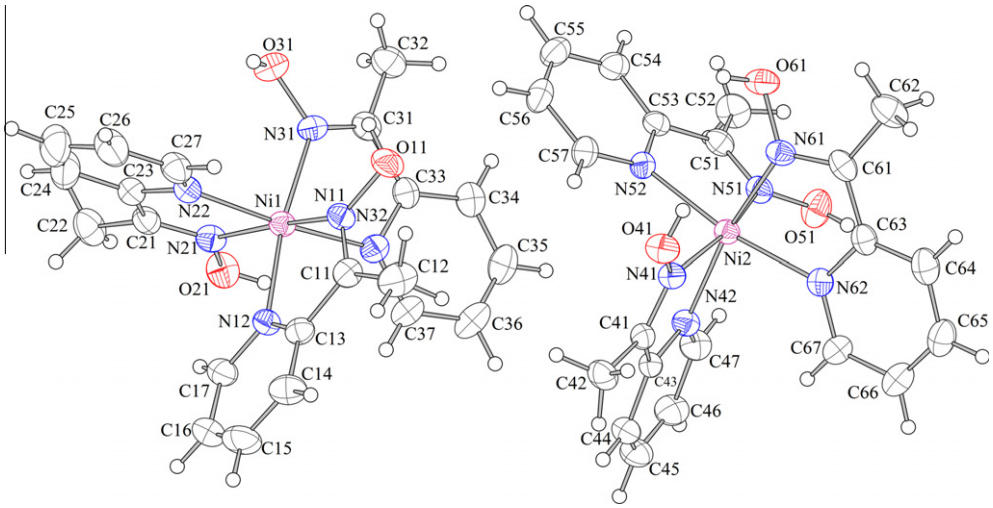

Fig. 3. Molecular structure and labeling for the cationic complexes $[Ni(mpkoH)_3]^{2+}$ (I) and (II) at their relative positions in **3**·½H_2O. Ellipsoids are at 30% probability levels.

Table 2
Selected bond lengths (Å) and bond angles (°) for complexes **1, 2** and **3**·½H_2O.

Bond lengths for ***1***			
Ni(1)—O(31)	2.0442(8)	Ni(1)—N(21)	2.0670(8)
Ni(1)—O(41)	2.0632(7)	Ni(1)—N(11)	2.0793(8)
Ni(1)—N(12)	2.0662(9)	Ni(1)—N(22)	2.1003(8)
Bond angles for ***1***			
O(31)—Ni(1)—O(41)	86.56(3)	N(12)—Ni(1)—N(11)	77.65(3)
O(31)—Ni(1)—N(12)	174.23(3)	N(21)—Ni(1)—N(11)	165.30(3)
O(41)—Ni(1)—N(12)	89.45(3)	O(31)—Ni(1)—N(22)	93.09(3)
O(31)—Ni(1)—N(21)	90.52(3)	O(41)—Ni(1)—N(22)	179.56(3)
O(41)—Ni(1)—N(21)	102.92(3)	N(12)—Ni(1)—N(22)	90.92(3)
N(12)—Ni(1)—N(21)	94.43(3)	N(21)—Ni(1)—N(22)	76.82(3)
O(31)—Ni(1)—N(11)	98.14(3)	N(11)—Ni(1)—N(22)	90.80(3)
O(41)—Ni(1)—N(11)	89.50(3)		
Bond lengths for ***2***			
Ni(1)—N(12)	2.0521(19)	Ni(1)—N(11)	2.069(2)
Ni(1)—N(21)	2.059(2)	Ni(1)—O(4)	2.0701(17)
Ni(1)—N(22)	2.0610(19)	Ni(1)—O(1)	2.074(2)
Bond angles for ***2***			
N(12)—Ni(1)—N(21)	96.60(8)	N(22)—Ni(1)—O(4)	178.43(9)
N(12)—Ni(1)—N(22)	94.67(8)	N(11)—Ni(1)—O(4)	85.23(8)
N(21)—Ni(1)—N(22)	77.74(9)	N(12)—Ni(1)—O(1)	172.67(9)
N(12)—Ni(1)—N(11)	77.19(6)	N(21)—Ni(1)—O(1)	86.53(7)
N(21)—Ni(1)—N(11)	169.88(8)	N(22)—Ni(1)—O(1)	92.47(8)
N(22)—Ni(1)—N(11)	94.66(8)	N(11)—Ni(1)—O(1)	100.60(9)
N(12)—Ni(1)—O(4)	86.84(8)	O(4)—Ni(1)—O(1)	86.01(9)
N(21)—Ni(1)—O(4)	102.55(8)		
Bond lengths for ***3***·½H_2O			
Ni(1)—N(12)	2.0682(18)	Ni(2)—N(42)	2.0575(18)
Ni(1)—N(22)	2.0693(19)	Ni(2)—N(61)	2.0631(18)
Ni(1)—N(31)	2.0761(19)	Ni(2)—N(41)	2.0694(18)
Ni(1)—N(11)	2.0788(19)	Ni(2)—N(51)	2.0765(18)
Ni(1)—N(32)	2.0822(19)	Ni(2)—N(62)	2.0943(18)
Ni(1)—N(21)	2.0866(19)	Ni(2)—N(52)	2.0948(17)
Bond angles for ***3***·½H_2O			
N(12)—Ni(1)—N(22)	89.76(7)	N(42)—Ni(2)—N(61)	169.71(7)
N(12)—Ni(1)—N(31)	172.16(8)	N(42)—Ni(2)—N(41)	77.43(7)
N(22)—Ni(1)—N(31)	96.73(7)	N(61)—Ni(2)—N(41)	99.69(7)
N(12)—Ni(1)—N(11)	77.32(7)	N(42)—Ni(2)—N(51)	94.74(7)
N(22)—Ni(1)—N(11)	96.52(8)	N(61)—Ni(2)—N(51)	89.86(7)
N(31)—Ni(1)—N(11)	97.51(7)	N(41)—Ni(2)—N(51)	166.57(7)
N(12)—Ni(1)—N(32)	97.39(7)	N(42)—Ni(2)—N(62)	93.25(7)
N(22)—Ni(1)—N(32)	171.74(8)	N(61)—Ni(2)—N(62)	76.84(7)
N(31)—Ni(1)—N(32)	76.48(7)	N(41)—Ni(2)—N(62)	90.91(7)
N(11)—Ni(1)—N(32)	89.10(7)	N(51)—Ni(2)—N(62)	100.51(7)
N(12)—Ni(1)—N(21)	96.07(7)	N(42)—Ni(2)—N(52)	96.71(7)
N(22)—Ni(1)—N(21)	77.18(8)	N(61)—Ni(2)—N(52)	93.28(7)
N(31)—Ni(1)—N(21)	89.68(7)	N(41)—Ni(2)—N(52)	92.66(7)
N(11)—Ni(1)—N(21)	171.01(8)	N(51)—Ni(2)—N(52)	77.28(7)
N(32)—Ni(1)—N(21)	97.87(8)	N(62)—Ni(2)—N(52)	169.94(7)

Table 3
Hydrogen bonds for **1**, **2** and **3**·½H_2O (distances in Å and angles in °).

D—H···A	*d*(D—H)	*d*(H···A)	*d*(D···A)	∠(DHA)
1				
O(11)—H(11)···O(32)	0.91(2)	1.58(2)	2.4848(11)	178.3(19)
O(21)—H(21)···O(42)	0.904(19)	1.616(19)	2.5190(11)	176.0(18)
2				
O(11)—H(11)···O(3)	0.82	1.88	2.686(3)	166.6
O(21)—H(21)···O(6)	0.82	1.88	2.677(3)	162.5
3·½H_2O				
O(11)—H(11)···O(202)[a]	0.82	2.45	3.210(3)	154.3
O(11)—H(11)···O(203)[a]	0.82	2.08	2.810(3)	148.9
O(21)—H(21)···O(203)	0.82	2.07	2.757(3)	141.8
O(31)—H(31)···O(202)[a]	0.82	1.96	2.689(3)	146.9
O(41)—H(41)···O(101)	0.82	1.98	2.733(3)	152.3
O(41)—H(41)···O(102)	0.82	2.54	3.190(3)	136.6
O(51)—H(51)···O(302)[b]	0.82	2.10	2.854(3)	151.9
O(51)—H(51)···O(303)[b]	0.82	2.19	2.818(4)	133.1
O(61)—H(61)···O(102)	0.82	1.83	2.626(3)	162.1

[a] Symmetry operation: $x, -y + ½, z - ½$.
[b] Symmetry operation: $-x + 1, y - ½, -z + 3/2$.

Table 4
Selected geometric parameters as obtained by employing PBE1PBE/STMIDI (T = 298 K).

Complex	Bond lengths (Å)		Angles (°)	
1	Ni—N(11)	2.080	N(11)—Ni—N(12)	77.5
	Ni—N(12)	2.102	N(11)—Ni—N(21)	161.5
	Ni—N(21)	2.080	N(11)—Ni—N(22)	90.6
	Ni—N(22)	2.102	N(11)—Ni—O(31)	103.5
	Ni—O(31)	2.020	N(11)—Ni—O(41)	89.9
	Ni—O(41)	2.020	O(31)—Ni—O(41)	87.7
2	Ni—N(11)	2.065	N(11)—Ni—N(12)	77.6
	Ni—N(12)	2.079	N(11)—Ni—N(21)	173.0
	Ni—N(21)	2.065	N(11)—Ni—N(22)	97.8
	Ni—N(22)	2.079	N(11)—Ni—O(1)	95.8
	Ni—O(1)	2.025	N(11)—Ni—O(4)	89.3
	Ni—O(4)	2.025	O(1)—Ni—O(4)	84.0
3·½H_2O	Ni—N(12)	2.076	N(12)—Ni—N(11)	77.4
	Ni—N(11)	2.066	N(12)—Ni—N(22)	96.0
	Ni—N(22)	2.102	N(12)—Ni—N(21)	92.4
	Ni—N(21)	2.066	N(12)—Ni—N(32)	96.0
	Ni—N(32)	2.107	N(12)—Ni—N(31)	171.0
	Ni—N(31)	2.068	N(32)—Ni—N(31)	76.7
4[a]	Ni—N(1)	2.053 (2.048)	N(1)—Ni—N(2)	76.3 (76.91)
	Ni—N(2)	2.111 (2.095)	N(1)—Ni—N(3)	164.8 (166.64)
	Ni—N(3)	2.053 (2.039)	N(1)—Ni—N(4)	93.2 (93.3)
	Ni—N(4)	2.111 (2.101)	N(1)—Ni—Cl(1)	103.4 (101.72)
	Ni—Cl(1)	2.312 (2.4236)	N(1)—Ni—Cl(2)	86.4 (88.69)
	Ni—Cl(2)	2.312 (2.4039)	Cl(1)—Ni—Cl(2)	100.9 (93.560)

[a] Atom numbering and experimental values in parentheses taken from Ref. [13].

Table 5
Selected atomic charges from the NPA analysis by using PBE1PBE/STMIDI (T = 298 K).

Complex	Ni	N(12)	N(22)	N(11)	N(21)	X(1)	X(2)
1[a]	1.278	−0.502	−0.502	−0.154	−0.154	−0.708	−0.708
2[b]	1.242	−0.520	−0.520	−0.166	−0.166	−0.578	−0.578
3[c]	1.245	−0.525	−0.546	−0.224	−0.219	−0.538	−0.231
4[d]	1.191	−0.481	−0.481	−0.163	−0.163	−0.624	−0.624

[a] X(1) = O(31); X(2) = O(41).
[b] X(1) = O(1); X(2) = O(4).
[c] X(1) = N(32); X(2) = N(31).
[d] N(12), N(22), N(11), N(21), X(1) and X(2) corresponds to N(1), N(2), N(3), N(4), Cl(1) and Cl(2) respectively, in Ref. [13].

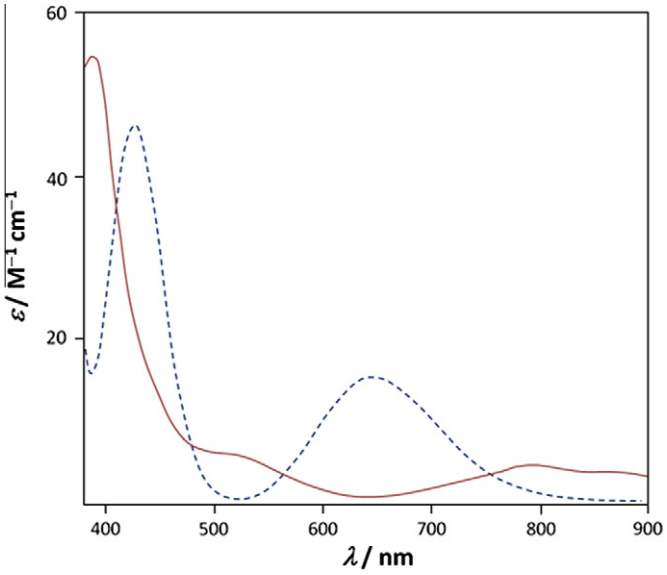

Fig. 4. Visible electronic absorption spectrum of **3** (broken line) calculated in CH_3OH by means of B3LYP/LANL2DZ (the one experimentally observed in solid line).

Table 6
Selected orbital excitations calculated for **3** in MeOH employing TD-B3LYP in combination with the LANL2DZ basis set.

Most important orbital excitations[a,b]	f	$\lambda_{calc.}$ (nm)	$\lambda_{exp.}$ (nm)	Origin[c]
H−14(β) → L+4(β), H−3(β) → L+3(β), H−3(β) → L+4(β)	0.0001	641.2	530	MLMLCT
H−11(β) → L+4(β), H−10(β) → L+4(β), H−6(β) → L+4(β)	0.0001	626.4		
H−11(β) → L+3(β), H−3(β) → L+3(β)	0.0003	425.5	395	MLMLCT
H−12(β) → L+4(β), H−4(β) → L+4(β)	0.0002	421.0		
H(α) → L+2(α), H(β) → L+2(β)	0.1770	281.5	Not observed	LLCT
H−4(α) → L+2(α), H−2(β) → L+2(β)	0.3168	275.5		
H−11(β) → L(β)	0.1114	223.7	Not observed	LLCT

[a] Only those excitation with contribution larger than 15% were considered.
[b] H = HOMO; L = LUMO.
[c] See in text for acronyms employed in assigning origin of absorption bands.

In going to the blue-part of the spectrum, a second low-intensity absorption band was experimentally identified for **1** and **3** at 396 and 395 nm, respectively. In both cases, the simulation also leads to a bathochromic shift of +34 and +28 nm, respectively. The corresponding bands for **2** and **4** are not seen, probably hided under the higher-absorptivity bands at this region of the spectrum.

For all complexes, the simulation also accounted for bands at the UV region (Figs. S4 and S5), which have not been detected experimentally due to solvent-absorption effects. In such cases, the theoretical results play an important role for the further understanding of the absorptive features of the complexes theoretically studied in all range of energy experimentally attainable. In all simulated spectra, two intense absorption bands have been found at about 280 nm and 220 nm. Their position and intensity show some degree of dependence on the complex, in some case being simulated as asymmetric bands due to the presence of shoulders [37].

The analysis of MOs is very important to gain insight into the origin of absorption bands. The absorption simulated at 634 nm for **3** has its origin in excitations from the HOMO−14(β), HOMO−11(β), HOMO−10(β), HOMO−6(β) and HOMO−3(β), the LUMO+3(β) and LUMO+4(β) being the destination MOs. The MOs implicated (Fig. 5) exhibit an important degree of charge delocalization over the nickel ion and the ligands. The electronic transitions then involve the electron transfer from HOMO orbitals that are strongly mixed metal-ligand in character, to also strongly mixed character LUMO orbitals. This kind of so-called MLMLCT or metal-ligand-to-metal-ligand charge transfer transitions have been described in other transition metal complexes [20,38] and explains the origin of the band at 530 nm observed in the spectrum of **3**. The situation does not differ significantly for the other complexes. In all of them, despite the different sets of donor atoms, an important charge delocalization among the metal center and the ligands can also be observed in those MOs implicated in the electronic transitions (Figs. S6–S8). Therefore, the origin of the band at the red region of the visible spectra can be ascribed to a MLMLCT in all cases.

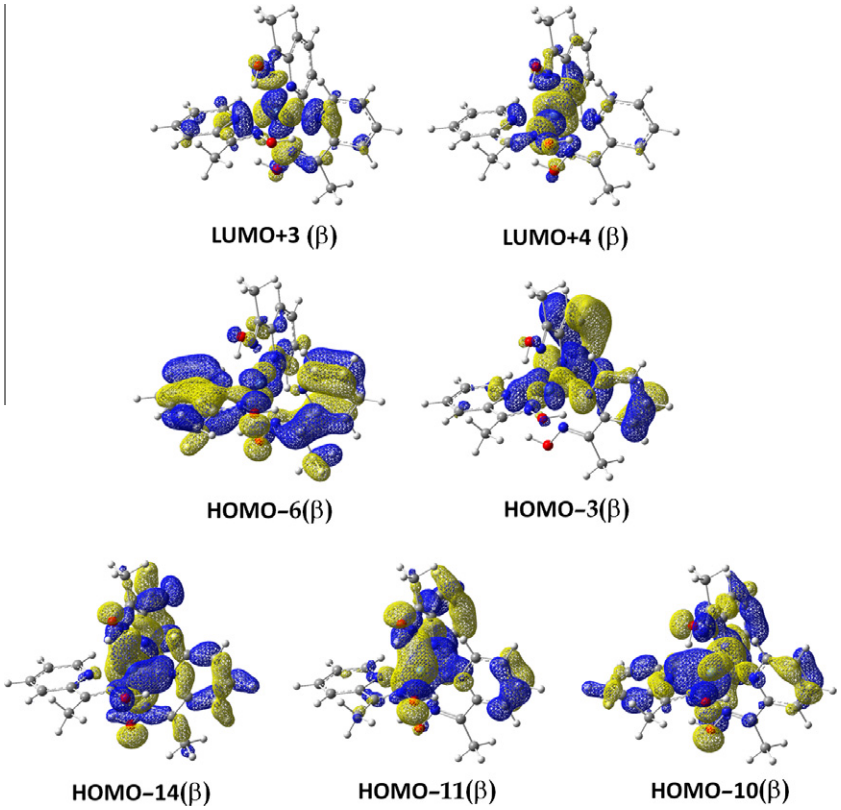

Fig. 5. HOMO- and LUMO-derivatives of **3** as obtained by employing B3LYP/LANL2DZ, involved in the origin of the shoulder experimentally observed at the low-energy part of the visible spectrum.

In analyzing the origin of the second low-intensity absorption band, the complex **2** has been excluded. For **3**, the charge moves from the HOMO−12(β), HOMO−11(β), HOMO−4(β) and HOMO−3(β) to the LUMO+3(β) and LUMO+4(β). In the case of **1**, the electronic density displaces from the HOMO−14(β) and HOMO−12(β) to the LUMO+5(β) and LUMO+7(β). The results for **4** show the charge being transferred from the HOMO−12(β), HOMO−3(β) and HOMO−2(β) to the LUMO(β), LUMO+1(β) and LUMO+5(β). The contours of the involved orbitals are depicted in Figs. S6–S8 and S9–S12. They allow us to assume a MLMLCT as origin of the band at about 400 nm.

The origin of the well-resolved bands simulated at the UV region of the spectrum can be also explained by means of the contours of the MOs involved. In all of them, the excitations lead mainly to a rearrangement of the charge density among the ligands, the contribution from metal-centered MOs playing a minor or even a negligible role. This finding allows assuming a ligand-to-ligand charge transfer (LLCT) as main origin of the bands simulated in the UV region of the spectra.

Concluding remarks

The reaction between $Ni(NO_3)_2{\cdot}6H_2O$ and mpkoH in methanol – with and without NaOOCPh – afforded crystals suitable for structure determination of three new Ni(II) compounds. All of these are mononuclear complexes in which the oxime ligands are protonated.

Their structural and electronic properties were studied by employing DFT methods, as well as for an analogous compound previously reported. The four complexes were theoretically investigated by means of PBE1PBE/STMIDI, a methodology we have found that can be employed with confidence for the investigation of nickel(II) complexes keeping the computational cost very low. The B3LYP/LANL2DZ method has proven to be also suitable in reproducing qualitatively the electronic UV–vis absorption spectra of the nickel complexes, enabling the explanation of the origin of the absorption bands experimentally observed.

Acknowledgements

This work was partially support by CSIC (Udelar, Uruguay) through Programa de Apoyo a Grupos de Investigación. L. Martinez is indebted to the Agencia Nacional de Investigación e Innovación (ANII, Uruguay) for a scholarship.

Appendix A. Supplementary material

Crystallographic data for the structural analysis have been deposited with the Cambridge Crystallographic Data Centre, CCDC reference numbers 861664–861666. A copy of this information may be obtained via http://www.ccdc.cam.ac.uk, or from the Cambridge Crystallographic Data Centre, 12 Union Road, Cambridge CB2 1EZ, UK; fax: (+44) 1223-336-033; or e-mail: deposit@ccdc.cam.ac.uk. Supplementary data associated with this article can be found, in the online version, at http://dx.doi.org/10.1016/j.saa.2012.12.042.

References

[1] R.B. Singh, B.S. Garg, R.P. Singh, Talanta 26 (1979) 425.
[2] D. Banerjea, K.K. Tripathi, Anal. Chem. 32 (1960) 1196.
[3] R.J. Thompson, R.H. Gore, F. Trusell, Anal. Chim. Acta 31 (1964) 590.
[4] C.G. Efthymiou, C.P. Raptopoulou, A. Terzis, S.P. Perlepes, A. Escuer, C. Papatriantafyllopoulou, Polyhedron 29 (2010) 627.
[5] C.G. Efthymiou, A.A. Kitos, C.P. Raptopoulou, S.P. Perlepes, A. Escuer, C. Papatriantafyllopoulou, Polyhedron 28 (2009) 3177.
[6] C. Papatriantafyllopoulou, G. Aromi, A.J. Tasiopoulos, V. Nastopoulos, C.P. Raptopoulou, S.J. Teat, A. Escuer, S.P. Perlepes, Eur. J. Inorg. Chem. 2007 (2007) 2761.
[7] T.C. Stamatatos, A. Escuer, K.A. Abboud, C.P. Raptopoulou, S.P. Perlepes, G. Christou, Inorg. Chem. 47 (2008) 11825.
[8] C. Papatriantafyllopoulou, M. Estrader, C.G. Efthymiou, D. Dermitzaki, K. Gkotsis, A. Terzis, C. Diaz, S.P. Perlepes, Polyhedron 28 (2009) 1652.
[9] C. Papatriantafyllopoulou, T.C. Stamatatos, C.G. Efthymiou, L. Cunha-Silva, F.A. Paz, S.P. Perlepes, G. Christou, Inorg. Chem. 49 (2010) 9743.
[10] C. Papatriantafyllopoulou, C.G. Efthymiou, C.P. Raptopoulou, A. Terzis, E. Manessi-Zoupa, S.P. Perlepes, Spectrochim. Acta A 70 (2008) 718.
[11] C. Papatriantafyllopoulou, C.P. Raptopoulou, A. Terzis, J.F. Janssens, S.P. Perlepes, E. Manessi-Zoupa, Z. Naturforsch. 62b (2007) 1123.
[12] K. Riggle, T. Lynde-Kernell, E.O. Schlemper, J. Coord. Chem. 25 (1992) 117.
[13] S. Mukherjee, B.A. Patel, S. Bhaduri, Organometallics 28 (2009) 3074.
[14] P. Chaudhuri, T. Weyhermüller, R. Wagner, S. Khanra, B. Biswas, E. Bothe, E. Bill, Inorg. Chem. 46 (2007) 9003.
[15] SAINT (version 7.68a), Area-Detector Integration Software, Bruker AXS Inc., Madison, USA, 2009.
[16] TWINABS (version 2008/4), Bruker AXS scaling for twinned, Bruker AXS Inc., Madison, USA, 2008.
[17] SADABS (version 2008/1), Bruker AXS area detector scaling and absorption correction, Bruker AXS Inc., Madison, USA, 2008.
[18] SHELXTL (version 2008/4), Bruker crystal structure solution and refinement, Bruker AXS Inc., Madison, USA, 2008.
[19] (a) J.P. Perdew, K. Burke, M. Ernzerhof, Phys. Rev. Lett. 77 (1996) 3865;
(b) C. Adamo, V. Barone, J. Chem. Phys. 110 (1999) 6158;
(c) A.D. Becke, J. Chem. Phys. 98 (1993) 5648.
[20] C. Pejo, H. Pardo, A. Mombrú, M.F. Cerdá, J.S. Gancheff, R. Chiozzone, R. González, Inorg. Chim. Acta 376 (2011) 105.
[21] J.S. Gancheff, P.A. Denis, E.F. Hahn, J. Mol. Struct. (Theochem) 941 (2010) 1.
[22] J.S. Gancheff, R.Q. Albuquerque, A. Guerrero-Martínez, T. Pape, L. De Cola, F.E. Hahn, Eur. J. Inorg. Chem. (2009) 4043.
[23] R.E. Easton, D.J. Giesen, A. Welch, C.J. Cramer, D.G. Truhlar, Theor. Chim. Acta 93 (1996) 281.
[24] (a) M. Dolg, U. Wedig, H. Stoll, H. Preuss, J. Chem. Phys. 86 (1987) 866;
(b) J.M.L. Martin, A. Sundermann, J. Chem. Phys. 114 (2001) 3408;
(c) D. Andrae, U. Häussermann, M. Dolg, H. Stoll, H. Preuss, Theor. Chim. Acta 77 (1990) 123.
[25] A. Bergner, M. Dolg, W. Kuechle, H. Stoll, M. Preuss, Mol. Phys. 80 (1993) 1431.
[26] (a) A.D. Becke, Phys. Rev. A 38 (1988) 3098;
(b) A.D. Becke, J. Chem. Phys. 98 (1993) 1372;
(c) C. Lee, W. Yang, R.G. Parr, Phys. Rev. B 37 (1988) 785.
[27] P.J. Hay, W.R. Wadt, J. Chem. Phys. 82 (1985) 299.
[28] P. Pyykkö, The Effect of Relativity in Atoms, Molecules and The Solid State, Plenum, New York, 1990.
[29] (a) V. Barone, M. Cossi, J. Phys. Chem. A 102 (1998) 1995;
(b) M. Cossi, N. Rega, G. Scalmani, V. Barone, J. Comp. Chem. 24 (2003) 669.
[30] N.M. O'Boyle, A.L. Tenderholt, K.M. Langner, J. Comp. Chem. 29 (2008) 839.
[31] (a) J.P. Foster, F. Weinhold, J. Am. Chem. Soc. 102 (1980) 7211;
(b) A.E. Reed, F. Weinhold, J. Chem. Phys. 83 (1985) 1736;
(c) A.E. Reed, R.B. Weinstock, B. Weinhold, J. Chem. Phys. 83 (1985) 735;
(d) A.E. Reed, L.A. Curtis, F. Weinhold, Chem. Rev. 88 (1988) 899.
[32] GAUSSIAN 03, Rev. D2, M.J. Frisch, G.W. Trucks, H.B. Schlegel, G.E. Scuseria, M.A. Robb, J.R. Cheeseman, J.A. Montgomery Jr., T. Vreven, K.N. Kudin, J.C. Burant, J.M. Millam, S.S. Iyengar, J. Tomasi, V. Barone, B. Mennucci, M. Cossi, G. Scalmani, N. Rega, G.A. Petersson, H. Nakatsuji, M. Hada, M. Ehara, K. Toyota, R. Fukuda, J. Hasegawa, M. Ishida, T. Nakajima, Y. Honda, O. Kitao, H. Nakai, M. Klene, X. Li, J.E. Knox, H.P. Hratchian, J.B. Cross, V. Bakken, C. Adamo, J. Jaramillo, R. Gomperts, R.E. Stratmann, O. Yazyev, A.J. Austin, R. Cammi, C. Pomelli, J.W. Ochterski, P.Y. Ayala, K. Morokuma, G.A. Voth, P. Salvador, J.J. Dannenberg, V.G. Zakrzewski, S. Dapprich, A.D. Daniels, M.C. Strain, O. Farkas, D.K. Malick, A.D. Rabuck, K. Raghavachari, J.B. Foresman, J.V. Ortiz, Q. Cui, A.G. Baboul, S. Clifford, J. Cioslowski, B.B. Stefanov, G. Liu, A. Liashenko, P. Piskorz, I. Komaromi, R.L. Martin, D.J. Fox, T. Keith, M.A. Al-Laham, C.Y. Peng, A. Nanayakkara, M. Challacombe, P.M.W. Gill, B. Johnson, W. Chen, M.W. Wong, C. Gonzalez, J.A. Pople, Gaussian, Inc., Wallingford CT, 2004.
[33] (a) H.D. Flack, Acta Cryst. A 39 (1983) 876;
(b) G. Bernardinelli, H.D. Flack, Acta Cryst. A 41 (1985) 500.
[34] (a) I. Bernal, Inorg. Chim. Acta 96 (1985) 99;
(b) L. Pérez-Garcia, D.B. Amabilino, Chem. Soc. Rev. 36 (2007) 941;
(c) F.E. Hahn, C. Schulze Isfort, T. Pape, Angew. Chem. Int. Ed. 43 (2004) 4807.
[35] I.J. Bruno, J.C. Cole, M. Kessler, Jie Luo, W.D.S. Motherwell, L.H. Purkis, B.R. Smith, R. Taylor, R.I. Cooper, S.E. Harris, A.G. Orpen, J. Chem. Inf. Comput. Sci. 44 (2004) 2133.
[36] A.B.P. Lever, Inorganic Electronic Spectroscopy, second ed., Elsevier, New York, 1986.
[37] An absorption band for 2, simulated as a shoulder peaked at 218 nm has been additionally observed (Fig. S8). It was originated mainly in two electronic excitations with contribution less than 15 % (at 218.5 nm with f = 0.0583, and at 218.3 with f = 0.0369) involving the HOMO–12(β), HOMO–11(α), HOMO–16(α), LUMO(β), LUMO+3(α), and LUMO+3(β).
[38] M. Al-Noaimi, M.A. AlDamen, Inorg. Chim. Acta 387 (2012) 45.